2024 IEEE/RSJ International Conference on Intelligent Robots and Systems (IROS)
October 14-18, 2024. Abu Dhabi, UAE

A Series Variable-stiffness Joint for Robot-assisted Resistance Training

Xingyu Hu, Yuebing Li, Haoyang Wu, Wuxiang Zhang, *Member, IEEE*, Yanggang Feng*, *Member, IEEE*

***Abstract*— As the safe and comfortable human-robot interaction draw more attention, variable stiffness joints are adopted in the rehabilitation robots for the compliant experiences. For patients with joint injury, resistance training has demonstrated its efficacy in concurrently enhancing muscle strength in the rehabilitation process. Here, we introduce a compact passive joint with variable stiffness and damping generation capability for robot-assisted resistance training. The abilities of serial variable stiffness and passive angle tracking were demonstrated by a prototype. The variable stiffness mechanism was mainly formed by 3D-printing, which only weighs 0.1kg with a wide range of stiffness (0.004-11.176Nm/rad). Moreover, the torque-angular displacement characteristics show excellent linearity at high joint stiffness. Finally, the feasibility of being integrated into the wearable rehabilitation robot has been evaluated.**

I. Introduction

Rehabilitation robots are widely used in rehabilitation practices for patients with joint injuries. Millions of people experience challenges in quality of daily life due to impairments of significant joints [1]–[3], *e.g.*, knee, ankle, elbow and shoulder. By providing assist forces or generating resistance forces for human locomotion, rehabilitation robots facilitate the increase of strength muscle strength and recruitment of nerves around the affected part [4], [5]. Traditional manual rehabilitation therapy makes it difficult to quantitatively evaluate the rehabilitation effect, and professional therapists' assistance and supervision are indispensable. Conversely, rehabilitation robots show advantages in terms of multiple work modes and precise motion parameter measurement [6].

Highly intensive human-robot interaction occurs in the working process of rehabilitation robots, in which highly rigid robotic joints are not appropriate. With the capability of preventing the human body from secondary injuries, compliant joints have emerged as more prominent approaches in rehabilitation practices relatively. In these days, variable stiffness mechanisms or variable stiffness actuators (VSAs) [7] show distinct advantages such as safer human-machine interaction [8], lower power consumption [9]–[11], and optimal energy storage ability [12], making them widely used in various robotic applications, *e.g.*, rehabilitation robots [13], [14] and compliant prostheses [15], [16]. Some of the VSAs based on lever mechanism can control the joint angular position and stiffness independently, which were proposed for improving operation range of motion (ROM) and stiffness adjustable ability [17]. It is considerable that the stiffness of VSAs based on moving the pivot can be changed from zero to infinity theoretically, which removes the limitation of inherent stiffness on the range of joint stiffness.

Portable and wearable rehabilitation robots with low weight gather more and more attention. Different from conventional devices with huge sizes and stationary bodies, wearable robots remove the obstacles of lower energy costs and home-based rehabilitation. Furthermore, with the support of intelligent terminals and remote diagnosis technology, wearable rehabilitation robots have the potential to pave the way for alleviating the problems of high medical costs and scarce medical resources.

In general, active motion is recommended to fight against the muscle atrophy caused by prolonged rest. For example, resistance training is an effective method for enhancing the strength of muscle groups during the rehabilitation process [18]–[20], which meets the application scenario of damping generation from the passive joint. Various damping joints were developed for active motion rehabilitation [21], but they are too bulky and heavy to wear without serial variable stiffness [6], [21]–[23].

To address the problems mentioned above, an integrated passive joint with variable stiffness and damping generation capability for wearable rehabilitation robots was proposed. As the joint illustrated in Fig. 1(a), a BLDC (brush-less direct-current) motor is applied for generating damping when back-driving the rotor, with a variable stiffness mechanism (based on adjusting the lever ratio) connected in series. A gear with Archimedes spiral grooves works as the compliant element of the variable stiffness mechanism. A theoretical model was established for evaluating the characteristics of the variable stiffness mechanism. Subsequently, the actual range of the joint was calibrated and the damping generation was validated with a joint angle tracking experiment carried on. The joint weighs only 0.56kg (the variable stiffness mechanism 0.1kg) with a high range of damping generation (peak resistance torque 12Nm) and high stiffness range (0.004-11.176Nm/rad).

II. Joint Design

A. Variable Stiffness Mechanism

The total structure of the proposed joint is shown in Fig. 1(a), in which two magnetic encoders and a torque sensor are integrated. A magnetic encoder is mounted on the frame of the variable stiffness mechanism for sampling angular displacement of the main arm, and another encoder is connected to the BLDC motor (Xiaomi Inc., reduction ratio 7.75:1) for rotor angle sampling. Apart from that, the

This research is supported, in part by National Key R&D Program of China under grant No. 2022YFB4701200 and in part by the Fundamental Research Funds for the Central Universities (YWF-23-L-1205). (*Corresponding author: Yanggang Feng, yanggangfeng@buaa.edu.cn)

Xingyu Hu, Yuebing Li, Haoyang Wu, Wuxiang Zhang, and Yanggang Feng are with the School of Mechanical Engineering and Automation, Beihang University.

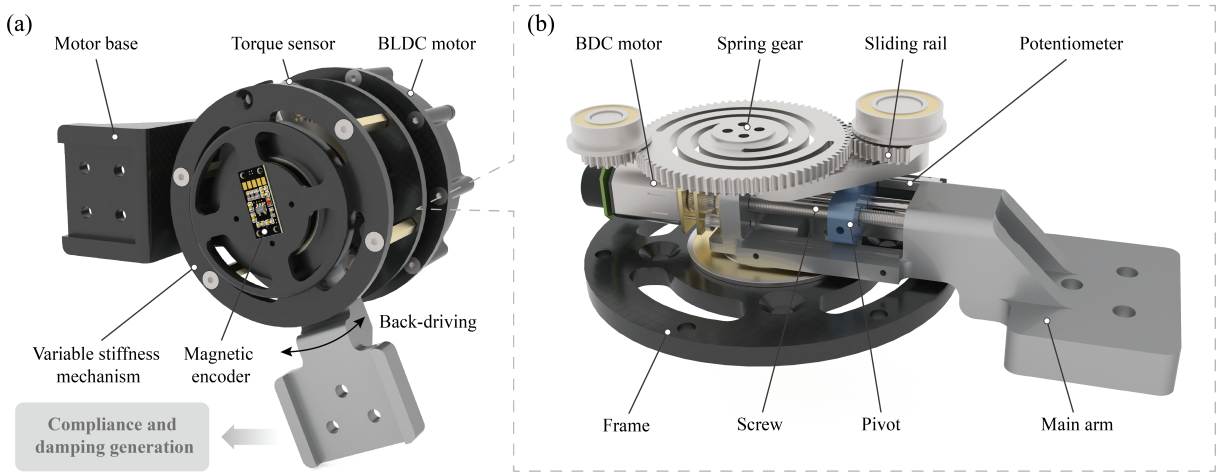

Fig. 1. Overview of the variable stiffness joint. (a) Joint components. The joint consists of a BLDC motor, a motor base and a variable stiffness mechanism with magnetic encoders and torque sensor. Variable stiffness and damping are generated while backing-driving the joint. (b) Structure of the variable stiffness mechanism. With the elasticity provided by a spring gear, the variable stiffness is realized by the adjustable transmission ratio (position of pivot).

torque sensor works as an adapter between the motor and the variable stiffness mechanism, and tracks joint torque in real time.

The detailed structure of the variable stiffness mechanism is illustrated in Fig. 1(b), which mainly consists of a main arm, a pivot, a spring gear, a sliding rail and two frames. The main arm and the frame form a hinge making the former capable of rotating around the frame. On another frame, a sliding rail with a groove (for pivot sliding) is mounted for load transmission, and its teeth segment (40 teeth, module 0.5mm) is in mesh with the spring gear (80 teeth). Due to the contribution of a screw (M3) and a macroprism (Φ3mm), the position of the pivot can be adjusted by rotating the screw using a BDC (brush direct-current) motor.

The spring gear was formed by 3D-printing using 6061 aluminum alloy, whose elasticity is brought by two hollow Archimedes spiral grooves (1.2 cycles, width 1.5mm). Except for the spring gear and standard parts, other parts are all formed by 3D-printing using PLA-CF materials (polylactic acid with carbon fibers). To prevent the spring gear from distortion during deforming, a small pinion gear (20 teeth) is mounted to be in mesh with the spring gear as shown in Fig. 2(a). To be noted, a potentiometer is placed on the main arm for sampling the position feedback of the pivot. At the condition of the same angular displacement for the main arm, the transmission ratio of the mechanism changed relevantly because of the movement of the pivot position (Fig. 2(b)).

B. Theoretical Stiffness Model

As shown in Fig. 2(a), the rotating center of the main arm, the geometric center of the pivot and the rotating center of the sliding rail are represented by points A, B and C, respectively. For the lever system, the distance between points A and B is defined as l, and the length of line segment AC is denoted as l_0 (25mm). The pivot can slide along the groove on the sliding rail. When the length of line segment AB is close to zero, the joint becomes softer, whose limit is that the main arm can rotate freely and the spring gear not deforms. Conversely, the main arm is fixed (degree of freedom is zero) when AB is equal to l_0 or B and C superpose each other, as a result, the theoretical joint stiffness is infinite.

Assuming all parts are rigid except for the spring gear, points A, B and C form a triangle that is shown in Fig. 2(b) when a load is exerted on the main arm. The angular displacement of the main arm and the sliding rail are denoted as θ and θ_1 respectively, and angular deformation of the spring gear is denoted as θ_2. According to the cosine theorem, the length of BC (denoted as d) can be calculated by the following equation:

$$d^2 = l^2 + l_0^2 - 2ll_0\cos\theta \tag{1}$$

Then θ_1 can be represented by l, l_0 and θ using the sine theorem:

$$\frac{d}{\sin\theta} = \frac{l}{\sin\theta_1} \tag{2}$$

$$\theta_1 = \arcsin\frac{l\sin\theta}{\sqrt{l^2 + l_0^2 - 2ll_0\cos\theta}} \tag{3}$$

Because of the reduction ratio between the teeth segment of the sliding rail (z_1 = 40, module 0.5mm) and the spring gear (z_2 = 80), θ_2 can be represented by θ_2 as follows:

$$\theta_2 = \frac{z_1}{z_2}\theta_1 \tag{4}$$

Subsequently, the torque exerted on the main arm (M) can be calculated through the deformation (θ_2) and inherent stiffness (k) of the spring gear:

$$M = k\theta_2 = k\frac{z_1}{z_2}\arcsin\frac{l\sin\theta}{\sqrt{l^2 + l_0^2 - 2ll_0\cos\theta}} \tag{5}$$

By differentiating with respect to θ, the final instantaneous joint stiffness K_{the} can be arranged as:

$$K_{the} = \frac{dM}{d\theta} \tag{6}$$

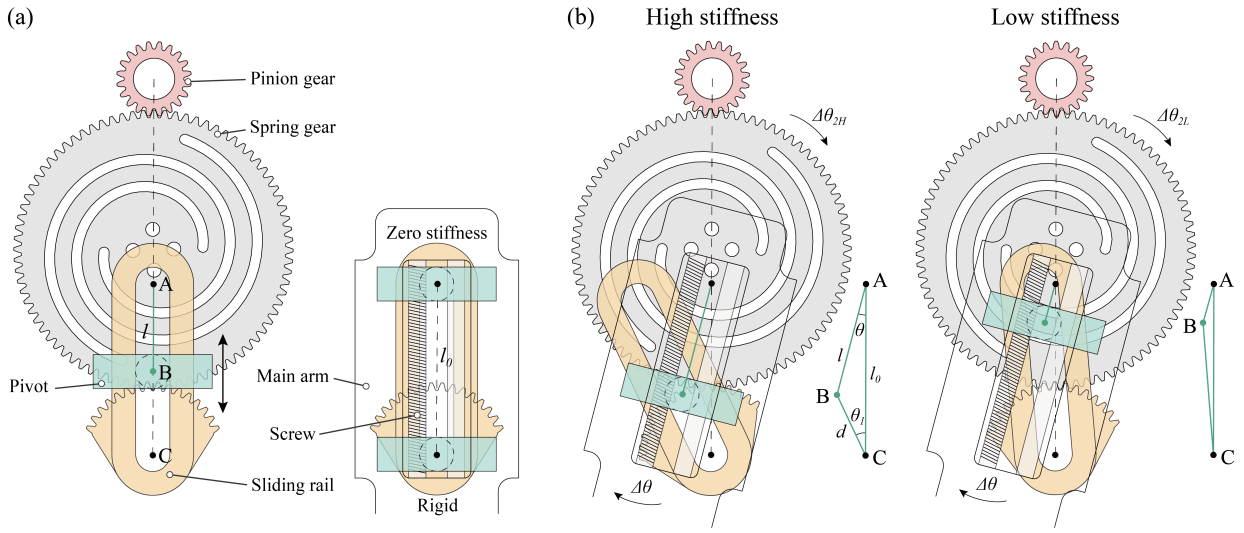

Fig. 2. Working principle of the variable stiffness mechanism. (a) Schematic of the mechanism. The position of the pivot (l) and angular displacement of the main arm (θ) dominate the joint stiffness, whose theoretical range extends from zero to infinity. (b) Working schematics at different stiffness. Same angular displacements $\Delta\theta$ are exerted on the main arm at low and high stiffness, angular deformation of the spring gear at high stiffness ($\Delta\theta_{2H}$) is bigger than it at low stiffness ($\Delta\theta_{2L}$).

$$K_{the} = k\frac{z_1}{z_2}\left(\frac{l\cos\theta\sqrt{l^2+l_0^2-2ll_0\cos\theta}}{\sqrt{\left(1-l^2\sin^2\theta\right)\left(l^2-2ll_0\cos\theta\right)}} - \frac{l^2 l_0\sin^2\theta}{\left(l^2+l_0^2-2ll_0\cos\theta\right)\sqrt{1-l^2\sin^2\theta}}\right) \tag{7}$$

From analyzing the model mentioned above, the joint stiffness is dominated by l and θ collaboratively. K_{the} is equal to zero when l is equal to zero, and K_{the} approaches infinity when l is equal to l_0.

C. Damping Generation

The BLDC motor is not used to rotate actively, *i.e.*, the rotor should be back-drived for damping generation. When an external load is exerted on the rotor, the three-phase windings of the BLDC motor are shortened together, *i.e.*, the plugging braking method [24], which has been proposed in our previous study. The back electromotive force obstructs the rotation of the rotor and generates damping simultaneously.

III. Calibration and Validation

Based on the theoretical stiffness model and mechanical structure, a control system and an experimental platform should be established for stiffness calibration and function validation of the joint prototype. The inherent stiffness of the spring gear and the stiffness of the total joint were calibrated by the platform mentioned above. To demonstrate the characteristics of damping generation, an passive angle tracking experiment was carried on.

A. Control system design

As shown in Fig. 3, a control circuit was developed for stiffness calibration and validation of damping generation. The core of the control and sampling system is a 32-bit microcontroller unit (MCU, STM32F405, STMicroelectronics). A lithium battery (Panasonic NCR18650, 3.7V) with a diameter of 18mm, a height of 66mm and a capacity of 3,800mAh is adopted as the main power. A boost circuit is used to convert the voltage input from the battery to a voltage of 12V. Considering the multiple needs for working voltage, a step-down chip (TPS54360DAR, Texas Instruments) is used to obtain a voltage of 5V to power the magnetic encoder and the torque sensor. The MCU is powered by a low dropout voltage regulator (AMS1117-3.3, Advanced Monolithic Systems) that generates a voltage of 3.3V based on the reference voltage of 5V.

The three-phase windings of the BLDC motor are connected to the inverter circuit (6 MOSFETs) integrated into the control circuit. The three-phase windings are connected to generate electromagnetic brake resistance by turning off/on all low (high-) side MOSFETs and turning on/off all high (low-) side at the same time. In this work, the 3 low-side MOSFETs are chosen as controlled plants and we maintain that the 3 high-side MOSFETs are turned off, thereby the turn-on time of the 3 low-side MOSFETs dominated the braking time of the motor. Adjusting the duty cycle of the PWM (Pulse Width Modulation) wave which drives the motor results in a change of damping magnitude directly.

The actual velocity of the joint is calculated according to the angle differentiation. A proportional-integral controller then processes the difference between the actual and desired velocities, and the control parameters (duty cycle of PWMs) are transmitted to the driver circuit in real time. A PWM generated by the MCU is received by a motor driver (DRV8323S, Texas Instruments), which communicates with the MCU through the serial peripheral interface (SPI) communication protocol to control the connection of the 3 low-side MOSFETs. Then the PWM is outputted from the

driver to the MOSFETs for braking the BLDC motor, *i.e.*, generating damping. Moreover, the BDC motor (12V) for stiffness adjusting is controlled by an RF module (Anntem, 433MHz), which can receive the signal from a remote control to drive the BDC motor.

B. Sensor signal sampling

The joint angle, the deformation and the joint torque are all sampled at a rate of 100Hz by the MCU. The magnetic encoders (TLE5012B, resolution 0.01°) for angle measurement are made by Infineon, and they communicate with the MCU through the SPI protocol with the angle data filtered in the MCU. The torque sensor (LZ-NJY54, 0-20Nm) is made by Hefei Lizhi Sensor System Co. Ltd., whose sensitivity is 0.8 ± 0.01mV/V. An operational amplifier (AD8221, Analog Devices) amplifies the differential signal of the torque sensor by 991 times for AD (analog to digital) sampling of the MCU.

The potentiometer (10KΩ) is powered by 3.3V power from the control circuit, and the voltage is measured by another AD channel for establishing a mapping with the pivot position (0-25mm) and corresponding one-to-one.

All data were collected by a PC software programmed with Java language (version 17), which has a graphical user interface (GUI) to communicate with the joint via WIFI (2.4GHz), and an oscilloscope panel is placed in the software interface for real-time observation of sensor signals (Fig. 3). The sensor signals that changed over time were packaged as files with the name extension, .mcvs, that were decoded and analyzed by MATLAB (version R2017b).

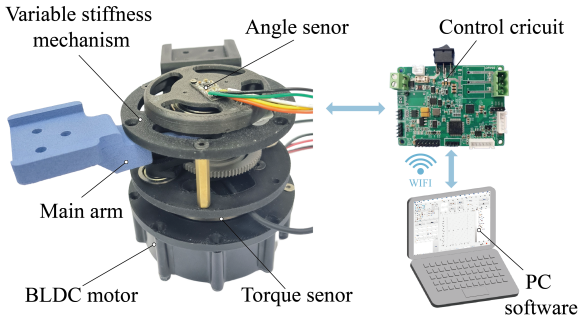

Fig. 3. Joint prototype and experimental platform. Though the control circuit, the joint angle, the deformation and the joint torque are measured by and the data are transmitted to the PC software via WIFI.

C. Inherent stiffness calibration of the spring gear

To build an experimental platform, the center of the spring gear was fixed to the torque sensor while a link was connected to the teeth of the spring gear. Then the motor base was fixed on the table and the rotor of the motor was locked. Finally, the link was swung 10 times in a range of -20° to 20° by hand. Through the PC software, the torque exerted on the gear and angular deformation of the spring (θ_2) were measured. As shown in Fig. 4(a), the scatters represent a linear correlation between the torque exerted on the teeth of the spring gear and the θ_2 apparently (correlation coefficient

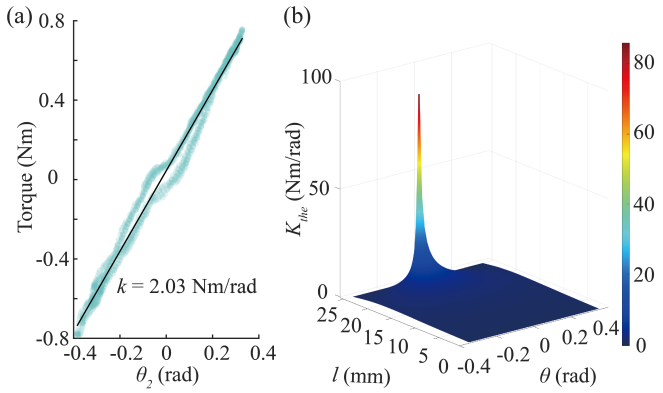

Fig. 4. Inherent stiffness characteristics of the spring gear. (a) Torque-angular deformation of the spring gear curve. Angular deformation of the spring gear is denoted as θ_2. (b) Theoretical stiffness model using the calibrated k (l = 0-24.9mm).

R = 0.993). The black solid line represents the linear fitting of torque and θ_2. Subsequently, the inherent stiffness k of the gear can be estimated by the slope of the fit line, which is 2.03Nm/rad. A hysteresis indicates that the spring gear undergoes slight plastic deformation under load.

By substituting the calibrated k into equation (7), the theoretical model of stiffness is illustrated. As shown in Fig. 4(b), the theoretical stiffness is approximately 85Nm/rad when l is 24.9mm and θ is 0°. It can be clearly seen in Fig. 4(b) that with the increase of l, the joint stiffness increases significantly when θ remains unchanged. The joint stiffness is 0Nm/rad when l is 0mm and the theoretical stiffness of the joint tends to infinity when l is close to l_0.

D. Joint stiffness calibration

After the inherent stiffness evaluation, another calibration was conducted to validate the stiffness characteristics of the joint. The motor base was fixed on the table and the rotor of the motor was locked. At different l, the torque exerted on the main arm and θ at different stiffness could be obtained. l was sequentially adjusted to 0, 5, 10, 15, 17, 18, 19, 21, 23 and 25mm, and the main arm was swung 10 times in each case under the external alternating motion. Similarly, the torque exerted on the main arm and θ were measured through the PC software. The calibration results are shown in Fig. 5.

As shown in Fig. 5(a), the linear relationship between torque and θ is not obvious when l is small by calculating the correlation coefficient R between torque and θ. The correlation coefficient R between torque and θ is 0.188 when l is 0mm. When l is greater than 10mm, the linear correlation between torque and θ is more significant. It can be clearly seen in Fig. 5(b) that with the increase of l, the joint stiffness increases obviously. When l is between 15mm-25mm, there is a significant change in joint stiffness. This is the reason for setting up multiple experiments between 15mm and 25mm. Theoretically, the stiffness of the joint is 0Nm/rad when l is 0mm, but the actual joint stiffness is 0.004Nm/rad due to friction. The joint stiffness reaches its maximum value of

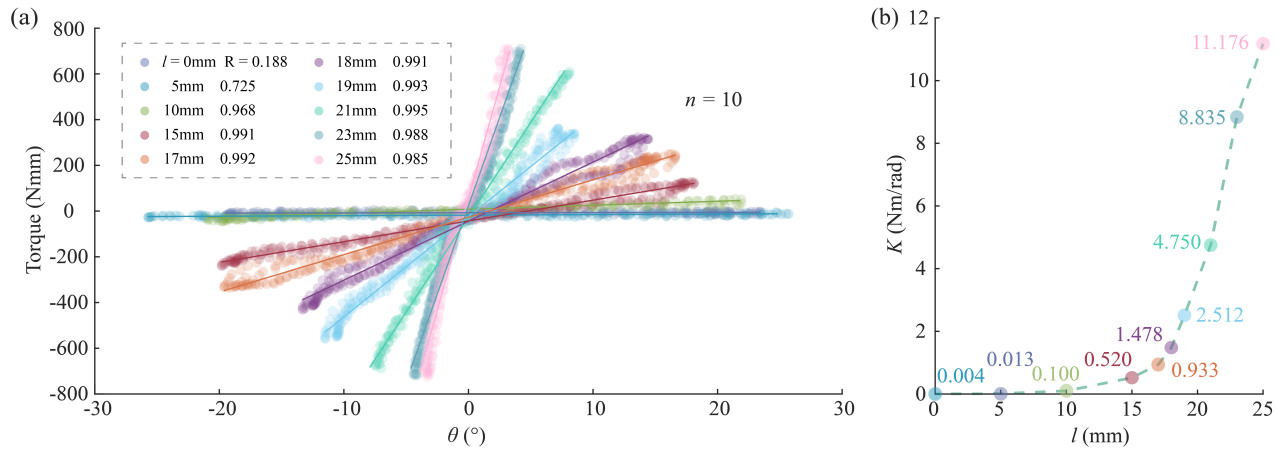

Fig. 5. Joint stiffness characteristics. Different colors represent different pivot positions. (a) Torque-angular displacement at different stiffness. The scatter of different colors represents the relationship between torque and θ at different l, the solid line represents the fitting line between the torque and θ whose color corresponds to the scatter. Angular displacement of the main arm is denoted as θ. Deformation repeated ten times (n = 10). (b) K - l curve. The color of scatter corresponds to (a), which represents the stiffness at different l.

11.176Nm/rad when l is 25mm. Moreover, it was observed that the joint stiffness does not change linearly with l and shows a nonlinear change with hysteresis, which is caused by the lever mechanism in the joint.

E. Joint angle tracking validation

To demonstrate the characteristics of damping generation, angle tracking experiments were carried on. At first, the pivot was placed at the maximum stiffness position(l = 25mm). Then the desired angular velocities were predetermined in the PC software, which are 60°/s, 90°/s and 120°/s. Joint angle is denoted as θ_j. Finally, the external alternating torque was exerted on the main arm and θ_j was measured by PC software.

As shown in Fig. 6, solid lines of different colors represent different desired angles and the dashed lines represent the actual angles. At three different angular velocities, the R squares between the actual angle and the desired angle are all greater than 0.96. This indicates that the desired angle curves fit well with the actual angle curves.

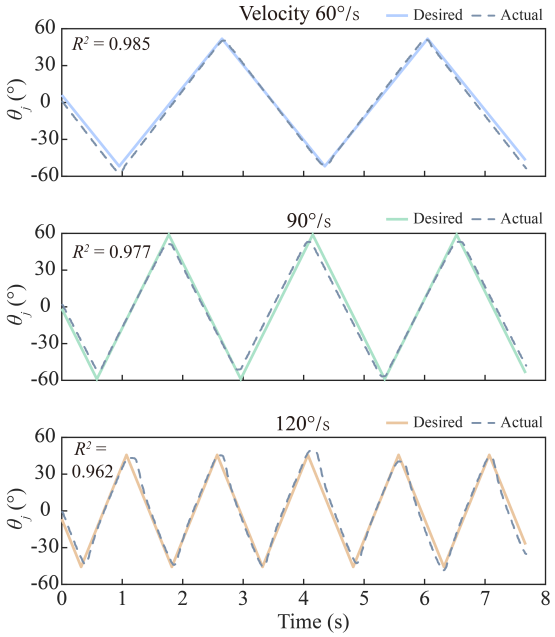

Fig. 6. Joint angle tracking at three velocities. The solid line and dashed line represents the desired angle and actual angle. With the external alternating torque, joints angle tracks the predetermined triangular waves.

IV. Discussion

Variable stiffness joints bring adjustable compliance to rehabilitation robots. By adjusting the inherent stiffness of the spring gear (Archimedes spiral parameters) and the transmission rate between the spring gear and the sliding rail reasonably, the shape of the K-l curve will show different characteristics. According to the theoretical stiffness model, the K_{the} decreases with the increase of the θ. Because of compensation by the incomplete linearity of the inherent stiffness shown in Fig. 4(a), the torque-θ curve shows excellent linear characteristics at high stiffness, and the coefficients of correlation (R) are all higher than 0.96 when l is equal to 10-25mm (Fig. 5(a)).

Because of the elasticity of the 3D-printing parts, the actual stiffness range of the prototype is from 0.004 (l = 0mm) to 11.176Nm/rad (l = 25mm), which is smaller than it calculated by the theoretical model. From another perspective, the maximum stiffness is more than three orders of magnitude greater than the minimum stiffness (the ratio is 2974), therefore the potential of a wide stiffness range is indicated. Subsequently, the accuracy of joint angle tracking (at constant velocities) caused by the antagonism between the joint damping and external torque was evaluated using R square. At three velocities, the R squares all exceed 0.96, which represents a fine similarity between the desired angle curve and the actual angle curve (Fig. 6).

For the application feasibility, the low weight and compact structure of the proposed joint make itself appropriate to be

used on wearable rehabilitation robots, that guarantee the portability and comfortable wearing experience. The wide stiffness range meets the needs of different rehabilitation stages with the capability of adjusting to the appropriate stiffness in resistance training. Notably, back-driving the motor along with energy regeneration [25], and harvesting energy from human locomotion to power the robotic system presents significance that can not be ignored. Consequently, more integrated design, wider range of variable stiffness and higher human-machine efficiency are targets that we are focusing on.

V. Conclusion

In pursuit of compliant and safe human-robot interaction during the robot-assisted resistance training, a compact joint with variable stiffness was proposed for the back-driving motion along with damping generation. The serial variable stiffness from 0.004 to 11.176Nm/rad was demonstrated by the torque and deformation data sampled from the prototype. We have validated a lightweight (0.1kg) variable stiffness mechanism with efficient space utilization (size 75*75*32.5mm) for more comfortable wearable experiences. Finally, external torque was exerted on the joint to verify the accuracy of passive angle tracking brought by the controllable damping, and the results show high precision characteristics at all velocities (60, 90 and 120°/s). Our future work will focus on enhancing the stiffness range and increasing the damping torque to be suitable for multiple scenarios. Furthermore, the energy efficiency will be optimized to meet the low power need for wearable robots.

References

[1] D. S. Logerstedt, D. A. Scalzitti, K. L. Bennell, R. S. Hinman, H. Silvers-Granelli, J. Ebert, K. Hambly, J. L. Carey, L. Snyder-Mackler, M. J. Axe *et al.*, "Knee pain and mobility impairments: meniscal and articular cartilage lesions revision 2018: clinical practice guidelines linked to the international classification of functioning, disability and health from the orthopaedic section of the american physical therapy association," *Journal of Orthopaedic & Sports Physical Therapy*, vol. 48, no. 2, pp. A1–A50, 2018.

[2] B. E. Smith, J. Selfe, D. Thacker, P. Hendrick, M. Bateman, F. Moffatt, M. S. Rathleff, T. O. Smith, and P. Logan, "Incidence and prevalence of patellofemoral pain: a systematic review and meta-analysis," *PloS one*, vol. 13, no. 1, p. e0190892, 2018.

[3] G. J. van Leeuwen, E. I. de Schepper, P. J. Bindels, S. M. Bierma-Zeinstra, and M. van Middelkoop, "Patellofemoral pain in general practice: the incidence and management," *Family Practice*, vol. 40, no. 4, pp. 589–595, 2023.

[4] B. A. Alkner and P. A. Tesch, "Knee extensor and plantar flexor muscle size and function following 90 days of bed rest with or without resistance exercise," *European journal of applied physiology*, vol. 93, pp. 294–305, 2004.

[5] H. Akima, K. Kubo, M. Imai, H. Kanehisa, Y. Suzuki, A. Gunji, and T. Fukunaga, "Inactivity and muscle: effect of resistance training during bed rest on muscle size in the lower limb," *Acta physiologica scandinavica*, vol. 172, no. 4, pp. 269–278, 2001.

[6] Q. Li, Y. Song, and D. Wang, "Damping control of rehabilitation robot for upper limbs," in *Proceedings of the 10th World Congress on Intelligent Control and Automation*. IEEE, 2012, pp. 3898–3902.

[7] S. Wolf, G. Grioli, O. Eiberger, W. Friedl, M. Grebenstein, H. Höppner, E. Burdet, D. G. Caldwell, R. Carloni, M. G. Catalano *et al.*, "Variable stiffness actuators: Review on design and components," *IEEE/ASME transactions on mechatronics*, vol. 21, no. 5, pp. 2418–2430, 2015.

[8] P. Bilancia, G. Berselli, and G. Palli, "Virtual and physical prototyping of a beam-based variable stiffness actuator for safe human-machine interaction," *Robotics and Computer-Integrated Manufacturing*, vol. 65, p. 101886, 2020.

[9] V. Chalvet and D. J. Braun, "Criterion for the design of low-power variable stiffness mechanisms," *IEEE Transactions on Robotics*, vol. 33, no. 4, pp. 1002–1010, 2017.

[10] L. C. Visser, R. Carloni, and S. Stramigioli, "Energy-efficient variable stiffness actuators," *IEEE transactions on robotics*, vol. 27, no. 5, pp. 865–875, 2011.

[11] A. Jafari, N. G. Tsagarakis, and D. G. Caldwell, "A novel intrinsically energy efficient actuator with adjustable stiffness (awas)," *IEEE/ASME transactions on mechatronics*, vol. 18, no. 1, pp. 355–365, 2011.

[12] J. Sun, Z. Guo, Y. Zhang, X. Xiao, and J. Tan, "A novel design of serial variable stiffness actuator based on an archimedean spiral relocation mechanism," *IEEE/ASME Transactions on Mechatronics*, vol. 23, no. 5, pp. 2121–2131, 2018.

[13] L. Liu, S. Leonhardt, C. Ngo, and B. J. Misgeld, "Impedance-controlled variable stiffness actuator for lower limb robot applications," *IEEE Transactions on Automation Science and Engineering*, vol. 17, no. 2, pp. 991–1004, 2019.

[14] B. Hu, B. Mao, S. Lu, and H. Yu, "Design and torque control base on neural network pid of a variable stiffness joint for rehabilitation robot," *Frontiers in Neurorobotics*, vol. 16, p. 1007324, 2022.

[15] M. K. Shepherd and E. J. Rouse, "The vspa foot: A quasi-passive ankle-foot prosthesis with continuously variable stiffness," *IEEE Transactions on Neural Systems and Rehabilitation Engineering*, vol. 25, no. 12, pp. 2375–2386, 2017.

[16] C. Everarts, B. Dehez, and R. Ronsse, "Variable stiffness actuator applied to an active ankle prosthesis: Principle, energy-efficiency, and control," in *2012 IEEE/RSJ International Conference on Intelligent Robots and Systems*. IEEE, 2012, pp. 323–328.

[17] A. Jafari, N. G. Tsagarakis, I. Sardellitti, and D. G. Caldwell, "A new actuator with adjustable stiffness based on a variable ratio lever mechanism," *IEEE/ASME Transactions on Mechatronics*, vol. 19, no. 1, pp. 55–63, 2012.

[18] D. Verrill, E. Shoup, G. McElveen, K. Witt, and D. Bergey, "Resistive exercise training in cardiac patients," *Sports Medicine*, vol. 13, no. 3, pp. 171–193, 1992.

[19] H. J. Hislop and J. Perrine, "The isokinetic concept of exercise," *Physical Therapy*, vol. 47, no. 2, pp. 114–117, 1967.

[20] H. G. Thistle, H. J. Hislop, M. T. Moffroid, and E. W. Lowman, "Isokinetic contraction: a new concept of resistive exercise." *Archives of physical medicine and rehabilitation*, vol. 486, pp. 279–82, 1967.

[21] G. Carpino, D. Accoto, M. Di Palo, N. L. Tagliamonte, F. Sergi, and E. Guglielmelli, "Design of a rotary passive viscoelastic joint for wearable robots," in *2011 IEEE International Conference on Rehabilitation Robotics*. IEEE, 2011, pp. 1–6.

[22] S.-M. Jeong, K.-S. Lee, and H.-S. Park, "Design of a variable damping mechanism for shoulder joint tracking device," in *2017 14th International Conference on Ubiquitous Robots and Ambient Intelligence (URAI)*. IEEE, 2017, pp. 683–685.

[23] X. Liu, H. Ji, H. Hu, and B. Xu, "Design and experimental analysis of knee joint of lower limb prosthesis based on magnetorheological damper," in *2022 7th International Conference on Intelligent Informatics and Biomedical Science (ICIIBMS)*, vol. 7. IEEE, 2022, pp. 168–172.

[24] J. Zhang, X. Liu, and Y. Feng, "Plugging energy regeneration improves braking torque at low speed instead of dynamic energy regeneration," in *2023 International Conference on Rehabilitation Robotics (ICORR)*. IEEE, 2023, pp. 1–5.

[25] Y. Feng, J. Mai, S. K. Agrawal, and Q. Wang, "Energy regeneration from electromagnetic induction by human dynamics for lower extremity robotic prostheses," *IEEE Transactions on Robotics*, vol. 36, no. 5, pp. 1442–1451, 2020.